

groundwater® week

Exhibits • Workshops • Summit

Las Vegas, Nevada • December 3-5, 2019

GROUNDWATER WEEK 2019 PROMOTES SCIENCE!

Hear the latest in groundwater research during presentations from scores of scientists and practitioners at this year's Groundwater Week.

Session topics range from emerging contaminants and managed aquifer recharge to groundwater remediation and sustainability — plus everything in between.

NGWA® The Groundwater Association

Irrigation ASSOCIATION®

Register: www.GroundwaterWeek.com

Groundwater

Electrical Resistivity Imaging of Seawater Intrusion into the Monterey Bay Aquifer System

by A. Pidlisecky[1], T. Moran[2], B. Hansen[3], and R. Knight[4]

Abstract

We use electrical resistivity tomography to obtain a 6.8-km electrical resistivity image to a depth of approximately 150 m.b.s.l. along the coast of Monterey Bay. The resulting image is used to determine the subsurface distribution of saltwater- and freshwater-saturated sediments and the geologic controls on fluid distributions in the region. Data acquisition took place over two field seasons in 2011 and 2012. To maximize our ability to image both vertical and horizontal variations in the subsurface, a combination of dipole–dipole, Wenner, Wenner-gamma, and gradient measurements were made, resulting in a large final dataset of approximately 139,000 data points. The resulting resistivity section extends to a depth of 150 m.b.s.l., and is used, in conjunction with the gamma logs from four coastal monitoring wells to identify four dominant lithologic units. From these data, we are able to infer the existence of a contiguous clay layer in the southern portion of our transect, which prevents downward migration of the saltwater observed in the upper 25 m of the subsurface to the underlying freshwater aquifer. The saltwater and brackish water in the northern portion of the transect introduce the potential for seawater intrusion into the hydraulically connected freshwater aquifer to the south, not just from the ocean, but also laterally from north to south.

Introduction

Groundwater is a critical component of freshwater supply systems throughout the globe (Alley et al. 2002), accounting for more than one-third of the water withdrawals worldwide (Doll et al. 2012). Heavy reliance on the resource has resulted in groundwater depletion of aquifers in many parts of the world and lead to a host of social, economic and environmental impacts including, reductions in surface water flows, the loss of groundwater-dependent ecosystems, and land subsidence (Wada et al. 2010). Coastal aquifers are particularly vulnerable to groundwater depletion, as overproduction of these systems can lead to seawater intrusion, which can cause degradation of water quality, and its subsequent loss as a source for drinking or irrigation (Bear et al. 1999).

In areas where there are concerns about seawater intrusion, monitoring wells are commonly installed to measure changing groundwater conditions and groundwater elevations. These monitoring wells, often referred to as sentinel wells, are intended to serve as an "early warning system" for seawater intrusion. However, well permitting, construction and monitoring can be time-consuming and expensive (Ogilvy et al. 2009). Additionally, individual monitoring wells provide point information, which may not be representative of groundwater conditions in the region as a whole. Effective management of coastal aquifers requires spatially continuous information that provides information on subsurface hydrogeology at a larger scale.

Geophysical techniques are commonly used to complement the spatially disparate information derived from borehole data and to help inform on the degree of heterogeneity surrounding the boreholes. Electromagnetic methods (EM; e.g., Kirkegaard et al. 2011; Jørgensen et al. 2012) and electrical resistivity tomography (ERT; Martínez et al. 2009; Nguyen et al. 2009; Henderson et al. 2010; de Franco et al. 2009) are well suited to characterization of saltwater intrusion, as they are sensitive to differences in subsurface conductivities (Goldman and Kafri 2006) resulting from changing salinity levels. However, care must be taken in the interpretation of results using electrical methods, as changing subsurface lithology, in particular changing clay content, can affect subsurface conductivities (Daily et al. 2004). To ensure accurate interpretation, geophysical methods should be combined with geophysical well logs (Buckley et al. 2001).

[1]Corresponding author: Department of Geosciences, University of Calgary, 2500 University Dr., Calgary, AB, Canada T2N 1N4; 403-220-6679; adampid@ucalgary.ca

[2]Water in the West, Stanford Woods Institute for the Environment, Stanford University, Stanford, CA 94305.

[3]Department of Geosciences, University of Calgary, Calgary, AB, Canada T2N 1N4.

[4]Department of Geophysics, Stanford University, Stanford, CA 94305.

Received September 2014, accepted May 2015.

doi: 10.1111/gwat.12351

Both marine- and land-based ERT have been proven to be successful methods of imaging various aspects of groundwater systems. Marine-based ERT surveys have been used to image groundwater discharge in coastal environments (Day-Lewis et al. 2006; Henderson et al. 2010). Land-based ERT surveys investigating freshwater/saltwater dynamics have also been widely used (Maillet et al. 2005; Batayneh 2006; Swarzenski et al. 2006; Martínez et al. 2009; Nguyen et al. 2009; de Franco et al. 2009) however few groundwater related surveys have been done at the scale of several kilometers (e.g., basin scale). However, large-scale (1–30+ km) land-based ERT surveys have been conducted recently in the petroleum and minerals industries, and there has been much development of field techniques to improve the acquisition speed of these surveys. Surveys of this length have much appeal for use in groundwater management because they have the potential to enable users to gain rapid insight into the subsurface lithology and fluid distributions over the full extent of an aquifer. However, there are particular challenges associated with using large electrode spacings. Two challenges of note are: (1) the amplitude of measured signals at long offsets (~1 km maximum spacing between outer electrodes) is small, and (2) the large arrays can be more sensitive to noise sources.

This study site overlies two groundwater basins on California's central coast, the Salinas groundwater basin and the Seaside groundwater basin (Figure 1). These groundwater basins are located in California's Monterey County, an agriculturally intensive region with an estimated annual production value of $4.4 billion (2013 values) (Monterey County Agricultural Commissioner [MCAC] 2013). Limited surface water resources in the area have placed tremendous pressure on the region's groundwater aquifers (approximately 86% of the region's water supply comes from groundwater; Department of Water Resources [DWR] 2013) and has resulted in seawater intrusion in many coastal aquifers surrounding Monterey Bay (Taraszki and Craig 2001; Hanson 2003; Hydrometrics 2009). We acquired data along a 6.8-km of data stretch of beach along the southern portion of Monterey Bay to: (1) demonstrate the viability of using large-offset ERT to image the distribution of subsurface freshwater and saltwater over a large spatial extent, and (2) gain insight in the distribution and geologic controls of seawater intrusion in the Monterey Bay region.

Study Area

Figure 1 shows the location of the 6.8 km of ERT data collected along the coast of Monterey Bay in 2011 and 2012. These data fall within two groundwater basins, the Salinas groundwater basin at the northern end of the transect and the Seaside groundwater basin to the south. The Salinas and Seaside groundwater basins are commonly delineated by a groundwater pumping-induced flow divide (Yates et al. 2005). The red line in Figure 1 represents this flow divide between the two basins. The

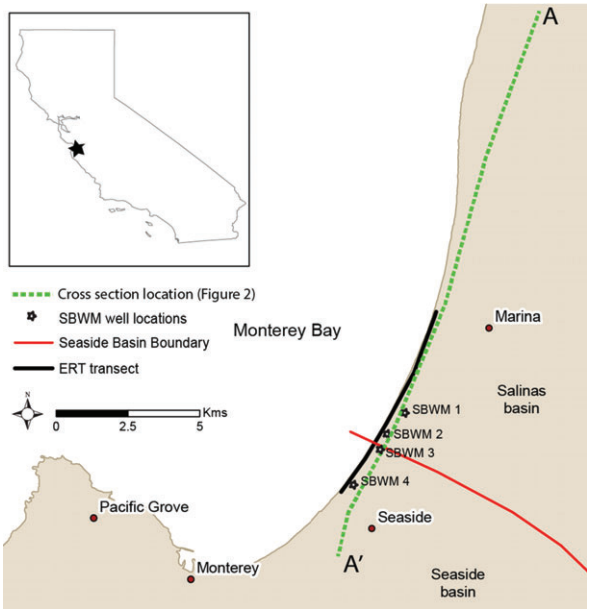

Figure 1. Map of field site location showing the ERT transect (heavy black line), Seaside basin water monitoring (SBWM) well locations (stars), the pumping-induced groundwater basin boundary (red line), and the location of a cross section of the region (dashed green line).

transect was performed in, and limited to, a permitted region within the California State park lands.

Seawater intrusion was first reported in the 1940's in the Salinas groundwater basin (Monterey County Water Resource Agency [MCWRA] 2006). Since that time, seawater intrusion of the shallower and deeper confined aquifers in the basin has advanced more than 11 and 6 km inland, respectively (MCWRA 2006). This has forced local water purveyors to drill groundwater wells into an alternate even deeper aquifer to meet local water demands.

Seawater intrusion has not yet been observed in the Seaside groundwater basin (Hydrometrics 2012). However, continued groundwater extractions in excess of freshwater inflows and recharge, pumping depressions near the coast and sustained seawater intrusion in the hydraulically connected Salinas River Basin suggest that seawater intrusion into the Seaside basin could occur (Hydrometrics 2012).

In 2007, four sentinel monitoring wells were installed along the coast of the Seaside and Salinas groundwater basins to provide for detection of seawater intrusion (Feeney 2007). We refer to these wells as Seaside Basin Water Monitoring (SBWM) wells.

Figure 2 is a conceptual model of the geology in the region developed by Feeney (2007). The cross section spans an approximately 20 km transect parallel to the coastline (green dashed line in Figure 1) and shows all strata dipping northward. Based on well logs from seven boreholes in the region, including the four SBWM wells, Feeney (2007) divides the strata in the region into two six main stratigraphic units, based on well logs from seven boreholes in the region, including the four SBWM wells. From oldest to youngest these units are (1) the Monterey

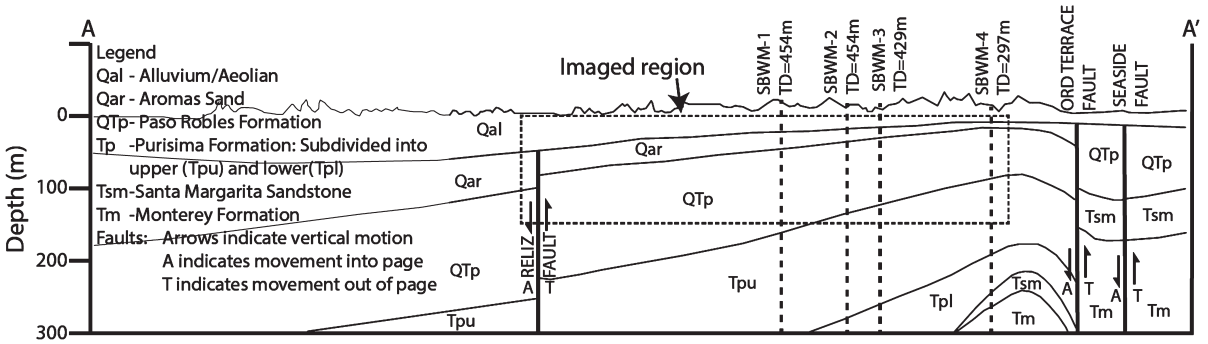

Figure 2. Cross section of geologic data along the southern coast of Monterey Bay (modified from Feeney 2007). The dashed box shows the length and approximate depth of the ERT data acquired for this study. The cross section is based on data from the four Seaside basin water monitoring (SBWM) wells shown in the cross section, as well as three additional wells that do not fall within our ERT transect and are not shown above. Total depth (TD) for each SBWM well is provided next to the well label.

Formation (Tm), (2) the Santa Margarita Formation (Tsm), (3) the Purisma Formation (Tpu and Tpl), (4) the Paso Robles Formation (QTp), (5) the Aromas Sand Formation (Qar), and (6) the Surficial deposits (Qal) (Durbin 2007).

Within these geologic formations are the three primary aquifers in the area. We refer to each by the geologic unit that houses them; they are the Aromas aquifer, the Paso Robles aquifer, and Purisma/Santa Margarita (PSM) aquifer. Because the Aromas aquifer is unconfined and in direct hydraulic communication with the ocean it is susceptible to contamination, and is, therefore, not considered a viable groundwater supply for the region (Yates et al. 2005). As a result, the Paso Robles and the PSM are the primary aquifers in the Seaside region.

The Salinas groundwater basin, north of SBWM 3, is a complex mix of hydraulically connected sand and gravel units inter-bedded among semi-continuous clay or silt units, resulting, fluvial and estuarine deposition from the Salinas River over time (Taraszki and Craig 2001). Furthermore, the interpretations by Taraszki and Craig (2001) suggest that the uppermost aquifers (surface 100 m) in the Salinas basin (north of north of SBWM 3) are hydraulically connected. Faulting and uplift in the southern portion of Monterey Bay have brought underlying deposits closer to the ground surface in the Seaside Basin, where the depth to the Monterey Formation (Tm in Figure 2), a marine shale and mudstone generally considered to be the base of water-bearing sediments in the region, is observed at a depth of approximately 280 m at the SBWM 4 (Yates et al. 2005). By contrast, the Monterey Formation is estimated at a depth of 500 m at SBWM 1 in the Salinas Basin. Interpretation of hydrogeologic data in this area is difficult and has resulted in conflicting interpretations of local lithology even when using data from the same boreholes (Yates et al. 2005). This is likely a result of several factors including, the complex depositional nature of the subsurface geology; the highly heterogeneous nature of the subsurface, making interpretation of the continuity of layers based on well data difficult and prone to error; and the vertical and horizontal displacement of layers resulting from faults (Merey et al. 1992).

Acquisition, Processing and Inversion of ERT Data

The ERT data were acquired along the beach, above the high tide line. Data were collected using two different acquisition systems. The dataset acquired in 2011 used a 200 W IRIS Syscal 72 electrode measurement system with an overall array length of 710 m. The 2012 data were collected using a 250-W IRIS Syscal 96 electrode system with an overall array length of 860 m. System segments were rolled over in 180 m segments during both field surveys to ensure continuous overlap in data acquisition. To maximize our ability to image both vertical and horizontal variations in the subsurface, a combination of dipole–dipole, Wenner, Wenner-gamma, and gradient measurements were made, resulting in a large final dataset of approximately 139,000 data points. The measurement quadruples had a range in geometric factors from approximately 18 m to 3.1×10^5m. The geometric factor is inversely proportional to the magnitude of the measured signal. This indicates that some of the measurements will be small (on the order of microvolts) and more susceptible to noise. Data acquisition took a total of 10 field days.

We adopted updated versions of the 2.5D forward modeling and inversion codes described by Pidlisecky and Knight (2008) and Pidlisecky et al. (2007). This code minimizes the objective function denoted in Equation 1, which results in an estimated electrical conductivity (EC) model that honors the measured data, while adhering to an a priori assumption regarding model structure (e.g., smoothness).

$$\begin{aligned}\phi(\mathbf{m}) = &\frac{1}{2}\left\|\mathbf{W}_{\mathrm{d}}\left(\mathbf{d}(\mathbf{m}) - \mathbf{d}_{\mathrm{obs}}\right)\right\|^2 \\ &+ \frac{\beta}{2}\left(\left\|\alpha_{\mathrm{s}}\mathbf{W}_{\mathrm{s}}\left(\mathbf{m} - \mathbf{m}_{\mathrm{ref}}\right)\right\|^2\right. \\ &\left. + \left\|\alpha_x \mathbf{W}_x(\mathbf{m})\right\|^2 + \left\|\alpha_z \mathbf{W}_z(\mathbf{m})\right\|^2\right) \qquad (1)\end{aligned}$$

where $\mathbf{m}$ is the natural log of the EC model, $\mathbf{d}_{\mathrm{obs}}$ is the observed data (the measured voltages normalized by

the injected current), $\mathbf{d}(\mathbf{m})$ is the data calculated for a given conductivity model, $\mathbf{W}_d$ is a data weighting matrix that contains $\frac{1}{\mathbf{std}(\mathbf{d_{obs}})+\mathrm{std}(\mathbf{d}(\mathbf{m}))+\mathrm{Pos}_{err}+\varepsilon}$ along the diagonal, $\mathbf{W}_s$ is a matrix that enforces smallness, $\mathbf{W}_x$ and $\mathbf{W}_z$ are matrices that enforce flatness in the x- and z-directions respectively, $\alpha_{s,x,z}$ are parameters that control the weighting of each regularization term, and β is a parameter that controls the overall weighting between regularization and data misfit. To form $\mathbf{W}_d$ we assume a random noise model of 3% for our observations ($\mathbf{std}(\mathbf{d_{obs}})$). We estimate the modeling error ($\mathbf{std}(\mathbf{d}(\mathbf{m}))$) by comparing numerical results to analytical solutions for a homogeneous conductivity structure. Positional error ($\mathbf{Pos}_{err}$) is calculated using the expected data error associated with a random positional error of 30 cm on the electrode positions (e.g., GPS error). We note that this positional error is particularly important when using mixed-array types, as different arrays have different sensitivity to positional error. Tidal variations were considered as a possible noise source; however, numerical modeling suggested this component would be negligible given the spatial scale of the survey and the relatively small tidal change (1 to 2 m). The final term, ε, in the error matrix serves to penalize small data values and was taken as 1e−5 (Oldenburg and Li 2005). We assume α_s is 1×10^{-4}, α_x is 10, α_z is 1, and β is 0.1. The starting model, or initial guess, for the inversion was a homogeneous model with an EC of 1.1 S/m (i.e., a saltwater-saturated sediment). The regularization term (β) was arrived at using the L-curve method (Hansen 1992). We note, for a comprehensive review regarding inversion, and the implications of these parameter choices, we refer the reader to the tutorial of Oldenburg and Li (2005). Resistivity data from the four SBWM wells (locations shown in Figure 1), while shown in the results, were not used to constrain the inversion. We chose not to constrain our inversion for two reasons: (1) integration of borehole logs as hard constraints (i.e., fixed model cells) in inversions can result in artifacts near the constrained region, and (2) using borehole data as soft constraints (e.g., using them to construct a starting model), can heavily influence the inversion result in regions where there is limited information content in the data (e.g., the inversion will not change the reference model).

Prior to inversion, data were removed based on several criteria: (1) an apparent resistivity of <0 Ohm-m or >300 Ohm-m, (2) positional error of >10%, and (3) modeling error >5%. The filtering resulted in a dataset with 120,848 points. Our results give an absolute mean percent error of 17.8%, after five iterations of the inversion algorithm. We note that this error value suggests our error assumption of 3% was low and that inversion error is higher than would typically be seen in surveys consisting of a single array type (e.g., Wenner). We attribute the higher error value to differences in sensitivity resulting from electrode position errors between the different arrays types, and the large spread in geometric factors. Studies often achieve better data fits by using data from a single array type. A complete Wenner survey along our transect would result in a total of approximately 30,000 data points, with geometric factors ranging from approximately 63 to 1800 m. This range in geometric factors results in data with a much lower noise floor, which could be fit to a tolerance of few percent; however, there would also be, limited information associated with this small dataset (larger geometric factors tend to provide information at greater depths). Working with multiple array types, while more challenging, results in a more detailed image with a greater depth of investigation.

Results and Discussion

Figure 3a through 3c shows data from the ERT survey as resistivity sections where the color displays the resistivity values. Resistivity sections in Figure 3a through 3c are hung at sea level along a digital elevation model for the region and show the locations of the four SBWM wells. These figures are shown from the perspective of looking inland from Monterey Bay; the digital elevation model provides insight into the topography of the area. We were able to obtain reliable results to a depth of approximately 150 m.b.s.l. along most of the resistivity section.

Figure 3a shows the inverted ERT data section overlain by the resistivity logs measured in each of the four SBWM wells. Logging data were not used to constrain the inversion of the ERT data, rather these data were used as an independent validation of the inversion. There is excellent agreement between the resistivity data derived from our inversion and the well log resistivity records. Minor variations in resistivity values between the records are attributed to differences in measurement scale.

As noted previously, interpretation of hydrogeologic data in this area is difficult and has resulted in conflicting interpretations of local lithology even when using data from the same boreholes (Yates et al. 2005). Geophysical methods may be particularly helpful in such environments, as they do not necessitate a complete understanding of the subsurface geology or mechanisms for their formation, rather they can be used to understand fluid distribution and potential flow paths within the existing geology. For example, in the absence of any other data, it is clear in Figure 3a that the geology is more laterally continuous in the southern portion, and that the seawater intrusion is vertically constrained. Using this information, we are able to infer the presence of a laterally continuous aquitard in the southern portion (3500 to 7000 m on the x-axis of Figure 3) of our transect.

Gamma logs are commonly used to identify differences in lithologic units, where high gamma counts are associated with zones of clay or high silt content and low gamma counts are associated with sands and gravels (e.g., Keys 1997). In Figure 3b, we use the resistivity data presented in Figure 3a in conjunction with the gamma logs from the SBWM wells to identify four dominant lithologic units within our depth section. These units are labeled A, B, C, and D and are consistent with the cross section shown in Figure 2. However, we do not go so far as to

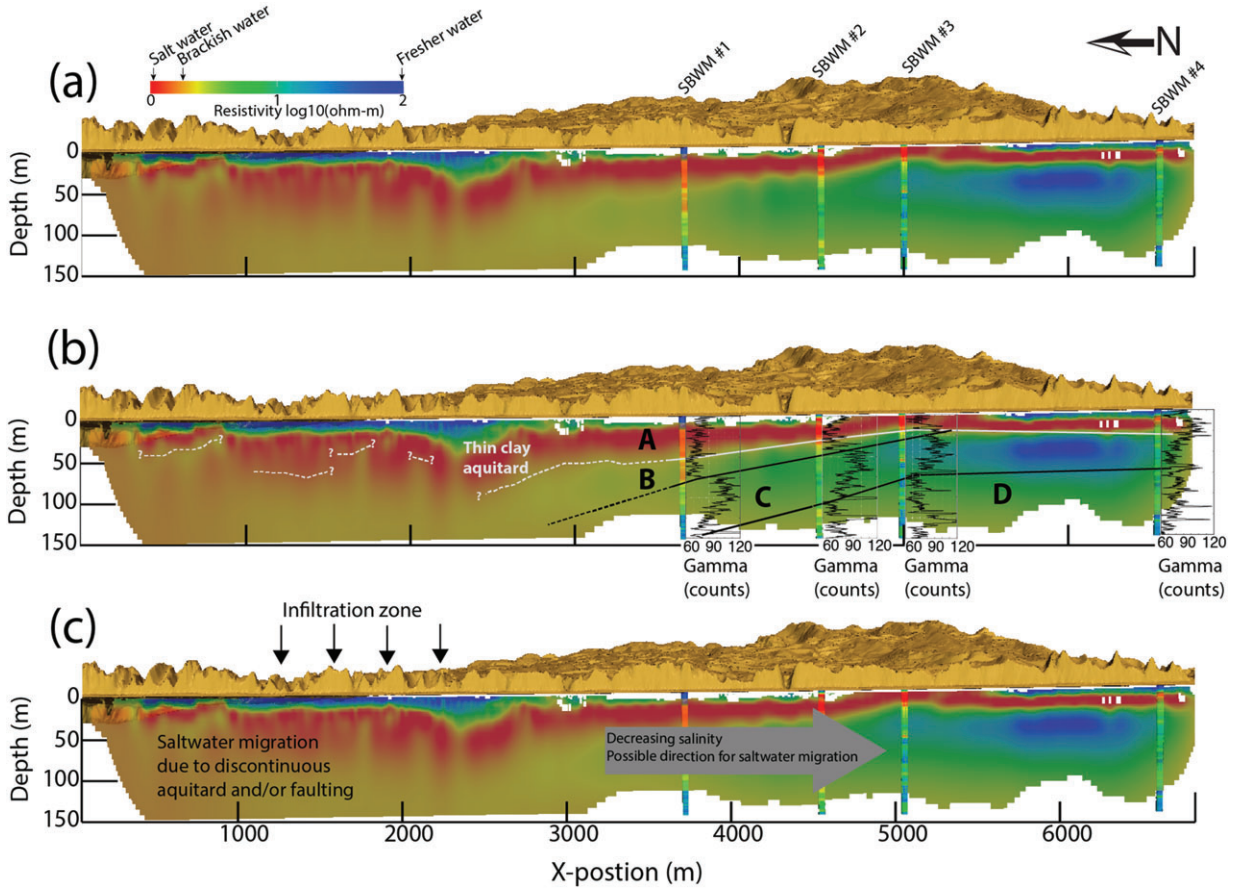

Figure 3. (a) Inverted electrical resistivity sections measured along the coast of Monterey Bay where color displays resistivity values. All sections are hung at sea level along a digital elevation model (DEM vertical exaggeration is 5×, data from the USGS national elevation dataset) for the region and are shown from Monterey Bay looking inland. All figures show the resistivity values measured in the SBWM wells (Feeney 2007). (b) Plots of gamma ray from the SBWM wells are shown. These data, along with the ERT and SBWM resistivity data, are used to identify four dominant lithologic units within our resistivity section, labeled A, B, C, and D. (c) We interpret the final image to show groundwater salinity and possible flow paths.

interpret the units labeled in Figure 3 using the names by Feeney (2007), rather we focus on interpreting them in terms of the data presented in Figure 3 (which gives no direct indication of age, or depositional environment).

Units A and B have similar and relatively consistent, low gamma count values, indicating a clean sand. However, based on the constrained nature of the saltwater layer observed in the southern portion (3500 to 7000 m on the x-axis of Figure 3) of the transect, along with the EC logs and spikes (>85 counts) in SBWM 1–4 gamma log records at depths of approximately 45, 34, 14, and 17 m, respectively, we interpret these as two different units separated by a thin clay aquitard (shown as a white line in Figure 3b). Unit C differs from units A and B by way of an increased gamma count within the unit, suggesting a higher average fines content. Unit D represents a transition back to a lower average gamma count, which we interpret as a higher sand fraction.

In the northern portion of our section, high salinity water dominates the upper third of the subsurface, suggesting the absence of a continuous aquitard in this portion of the section. We interpret this to mean the inferred clay layer in Figure 3b dips and becomes permeable (possibly due to faulting, thinning and/or erosion) in the northern portion (0 to 3500 m on the x-axis of Figure 3). These results are largely consistent with hydrogeologic interpretations by Taraszki and Craig (2001) who suggest that the uppermost aquifers (surface 100 m) in the Salinas basin are hydraulically connected, as well as with the ongoing problems of seawater intrusion that have been observed in the uppermost groundwater aquifers in the Salinas groundwater basin.

We note units B, C, and D are not yet intruded with saltwater, and that there is a freshwater zone in the southern portion of unit C (6000 m on the x-axis of Figure 3). This freshwater zone is consistent with depths reported for the Paso Robles aquifer (SBWM 3 40 to 130 m and SBWM 4 30 to 100 m) (Feeney 2007). This aquifer is a groundwater source for the overlying city of Seaside and is most likely recharged from precipitation falling on the uplands to the east. The interpretation is supported by the geologic interpretation of Yates et al. (2005), which suggests that inland exposure could be connected to Unit C. We also note that as the aquitard

between units A and B appears to be a less effective flow boundary (as evidenced by the decrease in resistivity due to increased salinity) toward the north and may indicate discontinuity in aquitards between the Salinas groundwater basin and the Seaside groundwater basin. Saline and brackish waters in the Salinas basin also introduce the possibility of seawater intrusion into units B, C, and D not just from the ocean, but also laterally from north to south. This is shown schematically in Figure 3c, with the flow arrow denoting the direction of possible saltwater migration.

There are two high resistivity anomaly (~50 to 100 Ohm-m) zones near the surface of our data section. These occur at 0 to 2500 m and 5500 to 7000 m on the x-axis of Figure 3. We interpret these as freshwater, likely due to infiltration from a series of drainage features that can be seen in the surficial topography of this region.

Conclusions

We use large-offset ERT to obtain 6.8 km of continuous electrical resistivity data to a depth of approximately 150 m.b.s.l. along the coast of Monterey Bay. Resistivity depth sections are combined with gamma logs records from coastal groundwater monitoring wells to infer the location of subsurface freshwater and saltwater zones. From these data, we are able to infer the existence of a contiguous clay layer in the southern portion of our transect. This layer prevents downward migration of the saltwater observed in the upper 25 m of the subsurface to the underlying freshwater aquifer. The clay layer dips northward in the northern portion of the line and becomes permeable, resulting in a downward migration of seawater to a depth of approximately 100 m. The saltwater and brackish water in the northern portion of the transect introduce the potential for seawater intrusion into the hydraulically connected freshwater aquifer to the south, not just from the ocean, but also laterally from north to south.

Finally, the resistivity data are used to identify a substantial infiltration zone near the surface (top 25 m) of the northern portion of our transect. We attribute this freshwater zone to be a result of series of drainage features along the coast. A similar, but smaller freshwater feature is observed in the southern portion of our transect and also coincides with a coastal drainages.

Understanding the impacts of subsurface lithology on fluid distribution and its potential flow paths is particularly important in coastal aquifers that are vulnerable to seawater intrusion. This study demonstrates the value of continuous data from large-offset ERT to delineate zones of subsurface freshwater and saltwater in a coastal environment. Resistivity data are used, in conjunction with gamma logs, to infer geologic controls on and potential contaminant pathways for seawater intrusion. Furthermore, the results from this study have demonstrated the value of ERT data to image subsurface freshwater and saltwater zones in this region and served as a proof-of-concept for a 48-km ERT from Seaside, California to Santa Cruz, California at the end of 2014.

Acknowledgments

The authors would like to thanks Curtis Ferguson, Jackie Randall, Nick Odlum, Andrew Parsekian, and Jan Walbrecker for their help in the field, as well as Ben Mirus and Kim Perkins from the United States Geologic Survey—Menlo Park who provided invaluable equipment support. We would also like to thank Stephen Bachmann from California State Parks—Monterey Division, and Tim Jensen from Monterey Peninsula Regional Parks for project support and coastal access. This work would not have been possible without financial support from the S. D. Bechtel, Jr. Foundation, and the Canadian Natural Sciences and Engineering Research Council. Additional financial and personnel support was received from Stanford University's Centre for Groundwater Evaluation and Management and personnel support was received from Stanford University's Water in the West Program. The authors wish to thank three anonymous reviewers for their suggestions and feedback for improving improve this manuscript.

Authors' Note: The authors do not have any conflicts of interest to report.

References

Alley, W.M., R.W. Healy, J.W. LaBaugh, and T.E. Reilly. 2002. Flow and storage in groundwater systems. *Science* 296, no. 5575: 1985–1990.

Batayneh, A.T. 2006. Use of electrical resistivity methods for detecting subsurface fresh and surface water and delineating their interfacial configuration: A case study of the eastern Dead Sea coastal aquifers, Jordan. *Hydrogeology Journal* 14, no. 7: 1277–1283. DOI:10.1007/s10040-006-0034-3.

Bear, J., A.H.-D. Cheng, S. Sorek, D. Ouazar, and I. Herrera (Eds). 1999. *Seawater intrusion in Coastal Aquifers—Concepts, Methods, and Practices*. Dordrecht, The Netherlands: Kluwer Academic Publishers.

Buckley, D.K., K. Hinsby, and M. Manzano. 2001. Application of geophysical borehole logging techniques to examine coastal aquifer palaeohydrogeology. *Geological Society, London, Special Publication* 189: 251–270. DOI:10.1144/GSL.SP.2001.189.01.15.

Daily, W., A. Ramirez, A. Binley, and D. LaBreque. 2004. Electrical resistance tomography. *The Leading Edge* 23, no. 5: 438–442.

Day-Lewis, F.D., E.A. White, C.D. Johnson, J.W. Lane Jr., and M. Belaval. 2006. Continuous resistivity profiling to delineate submarine groundwater discharge—Examples and limitations. *The Leading Edge* 25, no. 6: 724–728.

de Franco, R., G. Biella, L. Tosi, P. Teatini, A. Lozej, B. Chiozzotto, M. Giada, F. Rizzetto, C. Claude, A. Mayer, V. Bassan, and G. Gasparetto-Stori. 2009. Monitoring the saltwater intrusion by time lapse electrical resistivity tomography: The Chioggia test site (Venice Lagoon, Italy). *Journal of Applied Geophysics* 69, no. 3–4: 117–130. DOI:10.1016/j.jappgeo.2009.08.004.

Department of Water Resources (DWR). 2013. *California Water Plan—Update 2013: Chapter 3*, Vol. 1, 115. California Water Today. http://www.waterplan.water.ca.gov/docs/cwpu2013/Final/04_Vol1_Ch03_Ca_Water_Today.pdf.

Doll, P., H. Hoffmann-Dobrev, F.T. Portmann, S. Siebert, A. Eicker, M. Rodell, G. Strassberg, and B.R. Scanlon. 2012. Impact of water withdrawals from groundwater and surface water on continental storage variations. *Journal of Geodynamics* 59–60: 143–156.

Durbin, T.J. 2007. *Groundwater Flow and Transport Model—Seaside Groundwater Basin Monterey County, California*. Marina, California: RBF Consulting.

Feeney, M.B. 2007. *Seaside Groundwater Basin Watermaster Seawater Sentinel Wells Project*. Monterey, California: The Seaside Groundwater Basin Watermaster.

Goldman, M., and U. Kafri. 2006. Hydrogeophysical applications in coastal aquifers. In *Applied Hydrogeophysics, Proceeding of the NATO Advanced Research Workshop on Soils and Groundwater Contamination: Improved Risk Assessment*, ed. H. Vereecken, A. Binley, G. Cassiani, A. Revil, and K. Titov, 233–254. Dordrecht, The Netherlands: Springer.

Hansen, P.C. 1992. Analysis of discrete ill-posed problems by means of the l-curve. *SIAM Review* 34, no. 4: 561–580. DOI:10.1137/1034115.

Hanson, R.T. 2003. Geohydrologic framework of recharge and seawater intrusion in the Pajao Valley, Santa Cruz and Monterey Counties, California. U.S. Geological Survey Water-Resources Investigations Report 03-4096. Sacramento, California: U.S. Geological Survey.

Henderson, R.D., F.D. Day-Lewis, E. Abarca, C.F. Harvey, H.N. Karam, L. Liu, and J.W. Lane Jr. 2010. Marine electrical resistivity imaging of submarine groundwater discharge: sensitivity analysis and application in Waquoit Bay, Massachusetts, USA. *Hydrogeology Journal* 18, no. 1: 173–185. DOI:10.1007/s10040-009-0498-z.

Hydrometrics. 2012. *Water Year 2012: Seawater Intrusion Analysis Report Seaside Basin, Monterey County California*. Monterey, California: The Seaside Groundwater Basin Watermaster.

Hydrometrics. 2009. *Water Year 2009: Seawater Intrusion Analysis Report Seaside Basin, Monterey County California*. Monterey, Cambridge: The Seaside Groundwater Basin Watermaster.

Jørgensen, F., W. Scheer, S. Thomsen, T.O. Sonnenborg, K. Hinsby, H. Wiederhold, C. Schamper, T. Burschil, B. Roth, R. Kirsch, and E. Auken. 2012. Transboundary geophysical mapping of geological elements and salinity distribution critical for the assessment of future sea water intrusion in response to sea level rise. *Hydrology and Earth System Science* 16, no. 7: 1845–1862. DOI:10.5194/hess-16-1845-2012.

Keys, W.S. 1997. *A Practical Guide to Borehole Geophysics in Environmental Investigations*. Boca Raton, Florida: CRC Press, Inc.

Kirkegaard, C., T.O. Sonnenborg, E. Auken, and F. Jørgensen. 2011. Salinity Distribution in Heterogeneous Coastal Aquifers Mapped by Airborne Electromagnetics. *Vadose Zone Journal* 10, no. 1: 125–135. DOI:10.2136/vzj2010.0038.

Maillet, G.M., E. Rizzo, A. Revil, and C. Vella. 2005. High resolution electrical resistivity tomography (ERT) in a transition zone environment: Application for detailed internal architecture and infilling processes study of a Rhône River paleo-channel. *Marine Geophysical Researches* 26, no. 2–4: 317–328. DOI:10.1007/s11001-005-3726-5.

Martínez, J., J. Benavente, J.L. García-Aróstegui, M.C. Hidalgo, and J. Rey. 2009. Contribution of electrical resistivity tomography to the study of detrital aquifers affected by seawater intrusion-extrusion effects: The river Vélez delta (Vélez-Málaga, southern Spain). *Engineering Geology* 108, no. 3–4: 161–168. DOI:10.1016/j.enggeo.2009.07.004.

Merey, C., R. Miller, E. Ticken, and J. Lewis. 1992. Hydrogeologic characterization using a shallow seismic reflection survey at Fort Ord, California. In *62nd Annual International Meeting, SEG Expanded Abstracts*, New Orleans, LA, 370–373.

Monterey County Agricultural Commissioner (MCAC). 2013. *Monterey County Crop Report—2013*, 21. MCAC. http://ag.co.monterey.ca.us/download_resource/429.

Monterey County Water Resource Agency (MCWRA). 2006. *Monterey County Groundwater Management Plan*, 76. http://www.water.ca.gov/groundwater/docs/GWMP/CC-3_MontereyCoWRA_GWMP_2006.pdf

Nguyen, F., A. Kemna, A. Antonsson, P. Engesgaard, O. Kuras, R. Ogilvy, J. Gisbert, S. Jorreto, and A. Pulido-Bosch. 2009. Characterization of seawater intrusion using 2D electrical imaging. *Near Surface Geophysics* 7, no. 5–6: 377–390.

Ogilvy, R.D., P.I. Meldrum, O. Kuras, P.B. Wilkinson, J.E. Chambers, M. Sen, A. Pulido-Bosch, J. Gisbert, S. Jorreto, I. Frances, and R. Tsourlos. 2009. Automated monitoring of coastal aquifers with electrical resistivity tomography. *Near Surface Geophysics* 7, no. 5–6: 367–375.

Oldenburg, D.W., and Y. Li. 2005. Inversion for applied geophysics: A tutorial. In *Near-Surface Geophysics, Volume 1: Concepts and Fundamentals*, ed. D. Butler, 89–150. Tulsa, Oklahoma: Society of Exploration Geophysicists.

Pidlisecky, A., and R. Knight. 2008. FW2_5D: A MATLAB 2.5-D electrical resistivity modeling code. *Computers and Geosciences* 34, no. 12: 1645–1654. DOI:10.1016/j.cageo.2008.04.001.

Pidlisecky, A., E. Haber, and R. Knight. 2007. RESINVM3D: A 3D resistivity inversion package. *Geophysics* 72, no. 2: H1–H10. DOI:10.1190/1.2402499.

Swarzenski, P.W., W.C. Burnett, W.J. Greenwood, B. Herut, R. Peterson, N. Dimova, Y. Shalem, Y. Yechieli, and Y. Weinstein. 2006. Combined time-series resistivity and geochemical tracer techniques to examine submarine groundwater discharge at Dor Beach, Israel. *Geophysical Research Letters* 33, no. 24: L24405. DOI:10.1029/2006GL028282.

Taraszki, M., and D.J. Craig. 2001. Final report hydrological investigation of the Salinas Valley Basin in the vicinity of Fort Ord and Marina Salinas Valley, California. Harding ESE Project No. 51750 007. Salinas, California: Monterey County Water Resources Agency.

Wada, Y., L.P.H. van Beek, C.M. van Kempen, J.W.T.M. Reckman, S. Vasak, and M.F.P. Bierkens. 2010. Global depletion of groundwater resources. *Geophysical Research Letters* 37, no. 20: L20402. DOI:10.1029/2010GL044571.

Yates, E.B., M.B. Feeney, and L.I. Rosenberg. 2005. *Seaside Groundwater Basin: Update on Water Resource Conditions*. Monterey, California: Monterey Peninsula Water Management District.